Finite Element and Plate Theory Modeling of Acoustic Emission Waveforms

W. H. Prosser, M. A. Hamstad[+]*, J. Gary[+], and A. O'Gallagher[+]

NASA Langley Research Center

Hampton, VA 23681-0001

*University of Denver

Denver, CO 80208

[+]National Institute of Standards and Technology

Boulder, CO 80303

Submitted to the Journal of Nondestructive Evaluation - May, 1998

ABSTRACT

A comparison was made between two approaches to predict acoustic emission waveforms in thin plates. A normal mode solution method for Mindlin plate theory was used to predict the response of the flexural plate mode to a point source, step-function load, applied on the plate surface. The second approach used a dynamic finite element method to model the problem using equations of motion based on exact linear elasticity. Calculations were made using properties for both isotropic (aluminum) and anisotropic (unidirectional graphite/epoxy composite) materials. For simulations of anisotropic plates, propagation along multiple directions was evaluated. In general, agreement between the two theoretical approaches was good. Discrepancies in the waveforms at longer times were caused by differences in reflections from the lateral plate boundaries. These differences resulted from the fact that the two methods used different boundary conditions. At shorter times in the signals, before reflections, the slight discrepancies in the waveforms were attributed to

limitations of Mindlin plate theory, which is an approximate plate theory. The advantages of the finite element method are that it used the exact linear elasticity solutions, and that it can be used to model real source conditions and complicated, finite specimen geometries as well as thick plates. These advantages come at a cost of increased computational difficulty, requiring lengthy calculations on workstations or supercomputers. The Mindlin plat theory solutions, meanwhile, can be quickly generated on personal computers. Specimens with finite geometry can also be modeled. However, only limited simple geometries such as circular or rectangular plates can easily be accommodated with the normal mode solution technique. Likewise, very limited source configurations can be modeled and plate theory is applicable only to thin plates.

Key Words: Acoustic Emission, Plate Theory, Finite Element Modeling

INTRODUCTION

The ability to accurately model acoustic emission (AE) waveforms offers significant potential for improving the interpretation of AE data. Applications of such models include the determination of optimal placement of sensors in an AE test, the scaling of AE results from laboratory coupons to structures of practical interest, the calibration of transducers, and insight into inversion of AE data to eliminate extraneous noise and identify source mechanisms. However, in much of the early work [1-4] on modeling AE waveforms, approaches introduced in seismology have been applied to model the propagation of bulk and surface waves. Such models could be used to predict waveforms only in an infinite half-space, or in a plate of infinite lateral extent. In the plate geometry, the results were valid only for short propagation distances of less than ten plate thicknesses.

The geometries of many practical structures of interest for AE monitoring, though, are neither infinite in lateral extent, nor composed of thick plates or large components where

propagation of bulk waves is dominant. Thin plates, pipes, shells, rods, and beams are common. In such geometries, the distance from the receiver to the AE source is often many times the specimen thickness and the wave propagation is dominated by guided modes. Much experimental effort recently [5-10] has focused on guided wave propagation effects in the interpretation of AE signals. This research has led to improved accuracy in the locating the sources of emission, to the ability to better discriminate and eliminate extraneous noise signals, and to enhanced identification of AE sources.

Following this trend, recent theoretical efforts to model AE waveforms have also considered guided wave propagation. Integral transform techniques have been used to predict the Lamb wave response for AE sources in anisotropic composite materials [11-12]. Solutions were obtained for both exact elasticity theory and approximate laminated plate theory, and were shown to be in agreement with experimental observations. However, a limitation of this theoretical approach is that it again assumes a geometry of an infinite plate thus ignoring reflections from plate edges. A normal mode solution technique for classical plate theory has also been used to provide solutions for the flexural plate mode (lowest order antisymmetric Lamb mode) in plates with finite geometries [13]. Results for predictions of the flexural plate mode in an isotropic material were shown to agree with experimental observations of simulated AE signals for very low frequencies where this theory is valid. The extension of this solution technique to Mindlin plate theory (MPT) [14] which more accurately predicts the flexural plate mode at higher frequencies, is considered in this paper. Such an approach was also recently used for the prediction of flexural plate mode AE waveforms in isotropic plates and shown to be in agreement with experimental measurements of simulated AE signals [15]. In that work, solutions were also developed for the Mindlin-Medick plate theory to predict the extensional mode in isotropic plates as well. However, comparisons with exact linear elasticity solutions did not provide as good an agreement. A dynamic finite element method (DFEM) has been developed for predicting

AE waveforms in the far field in plates [16-17]. This approach also allows the consideration of plates of finite lateral extent. Theoretical predictions from this method were shown to be in good agreement with experimental measurements of signals generated by a simulated AE source.

In this research, theoretical predictions were compared from both DFEM and MPT for the flexural plate mode component of a simulated AE signal. Calculations were made with both isotropic (aluminum) and anisotropic (unidirectional graphite/epoxy) material properties. For the anisotropic material, several different directions of propagation were considered.

The DFEM has a number of advantages in that it is based on exact linear elasticity theory and can be used for both isotropic and anisotropic media. Additionally, the method has the potential to model realistic structural geometries to include propagation effects such as signal reflections. Realistic source geometries such as buried dipole sources can also be modeled. However, the DFEM calculations are computationally intensive requiring both significant memory and processor time. Currently, they can be made only on workstation or higher-class machines, and models take many hours or days to complete. The normal mode solutions to MPT are much less computationally demanding. They can be made on personal computers within minutes. Although both isotropic and anisotropic materials, as well as finite geometries, can be modeled, source configurations and specimen geometries which can be considered are limited. Also, MPT is an approximate theory and useful only for predicting the flexural mode response. Other plate theories, such as the Mindlin-Medick plate theory can predict the extensional mode, but typically do not provide as good an agreement with experimental measurements or predictions based on exact elasticity [15].

MINDLIN PLATE THEORY

Mindlin [14] improved on classical plate theory for isotropic media by including the effects of shear deformation and rotatory inertia. This approach was later extended to anisotropic laminated composites [18] and used to predict flexural mode dispersion [19] in composites. The normal mode solution technique of MPT used in this research was developed for predicting the response of an orthotropic laminated plate to an impact [20]. However, waves propagating away from the impact site were not considered in that work, as solutions were examined for the displacement only at the position of impact. More recently, the normal mode solution for MPT was used to model AE waveforms [15]. However, results only for isotropic materials were presented.

As the derivations of MPT and the normal mode solution approach are available in the references mentioned above, they are not repeated in detail here. A specially orthotropic composite laminate, which is a symmetric laminate with plies in the 0 and/or 90 degree directions only, is assumed with the *z* axis normal to the plate. The normal mode solution for the *z* axis displacement (*w*) is presented. The plate was assumed to be rectangular with a thickness (*h*), length (*a*) along the *x* axis, and width (*b*) along the *y* axis. Simply supported boundary conditions were assumed along the plate edges. The material properties were the density (ρ), the classical laminated plate bending stiffness coefficients (D_{11}, D_{12}, D_{22}, and D_{66}), and shear correction bending stiffnesses (A_{44} and A_{55}). A step function point load of amplitude *P* was assumed to occur on the plate surface at $x = \xi$, $y = \zeta$, and time, $t = 0$. The resulting displacement (*w*) at any point (*x*,*y*) as a function of time is then given by

$$w(x,y,t) = \frac{4P}{\rho hab} \sum_{n=1}^{\infty} \sum_{m=1}^{\infty} \frac{\sin \alpha_n x \sin \gamma_m y \sin \alpha_n \xi \sin \gamma_m \zeta (1 - \cos \beta_{nm} t)}{\beta_{nm}^2}, \quad (1)$$

where

$$\alpha_n = \frac{n\pi}{a}, \gamma_m = \frac{m\pi}{b}, \quad (2)$$

and

$$\beta_{nm}^2 = \frac{\omega_{nm}^2}{(1+\frac{\omega_{nm}^2}{E_{nm}^2})} \quad . \tag{3}$$

In Equation (3),

$$\omega_{nm}^2 = \frac{D_{11}\alpha_n^4 + D_{22}\gamma_m^4 + 2(D_{12} + 2D_{66})\alpha_n^2\gamma_m^2}{\rho h} \quad , \tag{4}$$

and

$$E_{nm}^2 = \frac{A_{44}\gamma_m^2 + A_{55}\alpha_n^2}{\rho h} \quad . \tag{5}$$

The term β_{nm} represents the frequency for the given normal mode. An approximate solution is obtained by calculating the summations up to given values of *n* and *m*. The resulting waveform then contains frequencies only up to the value of β_{nm} for these maximum values. For all calculations in this work, a total of $n = m = 200$ normal modes were summed.

For an isotropic material, the following relationships hold between the plate stiffness coefficients and the Young's modulus (*E*), Poisson's ratio (υ), and the shear modulus (*G*):

$$D_{11} = D_{22} = D = \frac{Eh^3}{12(1-\upsilon^2)} \quad , \tag{6}$$

$$D_{12} = \upsilon D = \frac{\upsilon Eh^3}{12(1-\upsilon^2)} \quad , \tag{7}$$

$$D_{66} = \frac{(1-\upsilon)}{2} D = \frac{(1-\upsilon)Eh^3}{24(1-\upsilon^2)} \quad , \tag{8}$$

and

$$A_{44} = A_{55} = k^2 Gh \quad , \tag{9}$$

where

$$G = \frac{E}{2(1+\upsilon)} \quad . \tag{10}$$

and κ is the shear correction coefficient. A value of 5/6 for κ^2 has been derived for materials which are homogeneous through the thickness of the plate [20]. This was the case for both the aluminum and the unidirectional graphite/epoxy modeled in this work.

DYNAMIC FINITE ELEMENT METHOD

The DFEM used in this research has been reported elsewhere [16,17] and the details are not repeated here. Both a two-dimensional, cylindrically symmetric model [16], which is useful for isotropic materials, and a three-dimensional model [17], which can handle anisotropic media, have been developed. The results from both models have been compared with experimental waveforms generated by simulated sources (pencil lead fractures) on a plate surface and acquired with an absolutely calibrated sensor. Model predictions and experimental measurements were in excellent agreement for isotropic materials. Because of the lower complexity and memory requirements of the two-dimensional approach, models can be run with either decreased cell size (increased spatial resolution) or much shorter calculation times. However, in addition to modeling anisotropic media, the three-dimensional approach is required to model realistic specimen geometries (other than a round plate with the source at the center) as well as realistic sources such as a non-axisymmetric buried dipole.

In both cases a leapfrog approximation in time and linear elements in space is used. Stress free boundary conditions are assumed along the top and bottom surfaces as well as along the outer edges of the plate. To model a step function in the DFEM, a linear ramp with rise

time smaller than the time step can be used. However, such a fast rise time can produce numerical transients in the calculated signal. For these calculations, the time step was approximately 0.02 μs while the rise time of the linear ramp source was 0.1 μs The effect of this rise time was evaluated by increasing it up to several microseconds in otherwise identical model calculations. For rise times of less than 1 μs, no differences were observed in the calculated flexural waveforms, which suggested that the linear ramp source with rise times over this range converged to a step function source for this mode. Likewise, the point source used in the plate theory calculations could not be modeled by the DFEM. The previous work has shown that the source diameter must be at least four time the cell dimension for sources with fast rise times to avoid introducing high frequency numerical transients. For all of these calculations, this minimum source size was used. For the high spatial resolution used in the two-dimensional model, this source diameter was quite small and approximated a point source well. As with the source rise time, the effect of the source diameter on the model results were evaluated by increasing the diameter up to several times the minimum value. Again, no effect was observed on the calculated waveforms. Because of the limited spatial resolution of the three-dimensional model, the minimum source diameter was larger. However, good agreement with the plate theory calculations was still observed.

ISOTROPIC MATERIAL (ALUMINUM)

The material properties for aluminum were used for both MPT and DFEM calculations. The density was assumed to be 2770 kg/m^3, Young's modulus to be 73.0 GPa, and Poisson's ratio to be 0.3. The plate thickness was taken as 3.175 mm. For MPT, a rectangular plate geometry was modeled with a length along x of 0.508 m and width along y of 0.381 m. The source was positioned at x = 0.254 m, y = 0.127 m. Five different receiver

positions were modeled, all along the x = 0.254 m line, at positions ranging from y = 0.2032 m to 0.3048 m at intervals of 2.54 cm. Thus, the distance from the source to the receiver varied from 7.62 cm to 17.78 cm (24 to 56 plate thicknesses). For the two-dimensional DFEM calculations, the radius was assumed to be 0.254 m, with the source positioned at the center of the plate (r = 0). The cell size, which was uniform in r and z, was 0.079 mm which provided 40 elements through the thickness. Again, five receivers were modeled at positions ranging from 7.62 cm to 17.78 cm in 2.54 cm intervals. So that only the asymmetric Lamb modes could be obtained from the DFEM results, simulated point receivers were placed both on top and bottom of the plate in the model. Then, by adding the signals from the top and bottom for a given location and dividing by two, the symmetric Lamb mode components were eliminated leaving only the asymmetric components. For both model calculations, the amplitude of the monopole source force function was assumed to be 1 N.

In Fig. 1, the model waveforms from both methods at propagation distances of 7.62, 12.7, and 17.78 cm are compared over a full 150 μs time scale. Overall, the agreement between the two methods is good. At longer times, there is some discrepancy between the signals, which was attributed to the effect of differences in reflections from plate edges. As the plate geometries and boundary conditions are different for the two methods, agreement in the prediction of reflected signals is not expected. The significant dispersion of this mode is observed when looking at the changes in the signal shape at different distances of propagation. Fig. 2 shows the same signals but at expanded time scales for the early arrival portion of the signals. More discrepancy between the two methods is observed for the higher frequencies in the early arrival. There are several possible explanations for these differences. The first could be the difference in the input force function between the step function used for MPT and the fast rise time linear ramp used for DFEM. However, the effect of varying the rise time was investigated and it is not believed that this is a significant

contribution to the differences. Another explanation could be the difference between the source diameter from the point source assumed in the plate theory model and the finite, but small, source used for the finite element calculations. Again, this was evaluated with the DFEM by varying the source diameter, with no significant changes observed. The final and most likely cause of the discrepancies is due to the approximate nature of MPT. Since the DFEM is based on exact linear elasticity and has been confirmed by comparison with experimental measurements, it is assumed that the differences observed are due to limitations of MPT.

ANISOTROPIC MATERIAL (GRAPHITE/EPOXY)

The composite material modeled was assumed to be a unidirectional material of thickness 2.54 mm. The elastic properties were assumed to be those of AS4/3502 graphite/epoxy. The axes were designated such that the *x* axis was along the fibers, the *y* axis was normal to the fibers in the plane of the plate, and the *z* axis was perpendicular to the plane of the plate. As a unidirectional material, the material was assumed to be transversely isotropic (nine nonzero elastic stiffness moduli, five of which are independent). The values of these coefficients, which were used in the DFEM calculations, are given in Table I. The coefficients used in the MPT calculations, which were calculated from the elastic properties in Table I, are shown in Table II.

Calculations were made for propagation along the fiber direction (0°), perpendicular to the fibers (90°), and at 45°. The three-dimensional DFEM model was used to include effects of anisotropy. This allowed the lateral geometry of a rectangular plate to be used for the DFEM and MPT models. However, it is noted that the boundary conditions along the edges were still different (stress free for finite element method and simply supported for plate theory). Thus, agreement at long times where significant reflection components are contained in the signals is not expected. Also, although the lateral plate dimensions were the

same for a given MPT and DFEM calculations for a particular propagation direction, they were not the same for all directions. This was because of the much larger memory requirements of the three-dimensional finite element method which placed limitations on the dimensions of the plate. For each direction, lateral dimensions, source location, and receiver positions were chosen to minimize the effects of reflections from the edges. For the 0° propagation direction, *a*, the lateral dimension along *x* was 0.254 m while *b*, the lateral dimension along *y* was 0.1524 m. For 90°, *a* was 0.1524 m and *b* was 0.254 m, and for 45°, *a* and *b* were both 0.2286 m. For all propagation directions, the distance from the source to receiver was varied from 7.62 to 15.24 cm (30 to 60 plate thicknesses) at intervals of 2.54 cm. However, results are shown only for a maximum propagation distance of 12.7 cm as the effect of reflections from the plate edges caused significant discrepancies at a distance of 15.24 cm. Again for the DFEM, the simulated point receivers were modeled both on top and bottom of the plate to allow elimination of the symmetric mode components in the signals.

For the DFEM, only ten elements were used through the thickness for a cell size of 0.254 mm. The cell aspect ratio was unity. This larger cell size was adequate for these calculations because of the low frequencies (and thus long wavelengths) in the flexural mode signals. However, because of the larger element size, there was a correspondingly larger source diameter which could have a minimum value of only four times the cell size. It is possible that this larger source diameter may have contributed to discrepancies between the DFEM results and those from MPT in which the point source was again used. As before, a linear ramp source with 0.1 μs rise time was used with an amplitude of 1 N.

The results for the DFEM and MPT models for propagation along the 0° direction at distances of 7.62 and 12.7 cm are shown in Fig. 3. Figures 4 and 5 show similar results for propagation along the 45° and 90° directions respectively. As these figures show, the

agreement is good. Some discrepancy due to differences in reflections is observed at later times in the waveforms.

SUMMARY AND CONCLUSIONS

Two theoretical methods for predicting flexural plate mode acoustic emission waveforms in thin plates were compared. The first was a dynamic finite element method (DFEM) and the second was based on a normal mode solution to Mindlin plate theory (MPT). Both methods were used to calculate the response of a plate to an out of plane source on the surface of a plate for both isotropic (aluminum) and anisotropic (unidirectional graphite/epoxy composite) materials. In general, good agreement between the two methods was observed. Discrepancies at long times in the waveforms were due to differences in the contributions from reflections from plate edges from different specimen geometries and/or boundary conditions for the two models. Since the DFEM is based on exact linear elasticity and has been previously verified by comparison with experimental measurements, the observed differences between the two techniques at shorter times, not caused by reflection differences, were attributed to the approximate nature of MPT.

Both methods allow calculations of waveforms in finite geometry specimens and can be used for isotropic and anisotropic media. However, since the DFEM is based on exact linear elasticity, it provides the displacements from all modes, symmetric and antisymmetric, while the MPT provides only the flexural plate mode (lowest order symmetric mode). Other plate theories can be used for the calculation of the extensional plate modes, but typically do not agree as well with experiment or full elasticity solutions. The DFEM can also be used to model arbitrary specimen geometries and source configurations, while MPT is limited to rectangular or circular geometries and much more limited source configurations. However, the trade-off for the enhanced capabilities of the DFEM is the significant computational intensity for this method. It requires workstation class computers

with significant memory and lengthy run times. The normal mode solution for MPT can be calculated on a personal computer in only a few minutes.

In discussing how these models might compare with signals generated by real AE sources in plates, it is noted that sources with a large out-of-plane or bending component generate preferentially large flexural plate modes. Such sources include impact, delamination in composites, and cracks near the surface or not symmetric with the midplane of the plate. Since both models predict the flexural mode response, they might both be applicable. Because of the flexibility in modeling different source configurations and geometries, the DFEM would obviously provide more accurate models for these real sources. However, in-plane sources such as fatigue cracking in metals and matrix cracking produce large extensional mode signals with little or no flexural modes if the crack is symmetric with respect to the midplane of the plate. For these real AE sources, MPT would not be useful as it does not predict the extensional mode.

REFERENCES

1. F. R. Breckenridge, Carl E. Tschiegg, and M. Greenspan, Acoustic Emission: Some Applications of Lamb's Problem, *J. Acoust. Soc. Am.* **57(3):**626-631 (1975).

2. N. N. Hsu, Dynamic Green's Functions of an Infinite Plate - A Computer Program, *NBSIR 85-3234* (1985).

3. Y. H. Pao, Theory of Acoustic Emission, *Elastic Waves and Non-Destructive Testing of Materials, AMD* **29**:107-128 (1978).

4. M Ohtsu and K. Ono, The Generalized Theory and Source Representations of Acoustic Emission, *J. Acoustic Emission*, **5(4)**:124-133 (1986).

5. M. R. Gorman, Plate Wave Acoustic Emission, *J. Acoust. Soc. Am.* **90(1)**:358-364 (1991).

6. M. R. Gorman and W. H. Prosser, AE Source Orientation by Plate Wave Analysis, *J. Acoustic Emission* **9(4)**: 283-288 (1991).

7. S. M. Ziola and M. R. Gorman, Source Location in Thin Plates Using Cross-Correlation, *J. Acoust. Soc. Am.* **90(5)**: 2551-2556 (1991).

8. M. R. Gorman and S. M. Ziola, Plate Waves Produced by Transverse Matrix Cracking, *Ultrasonics* **29**:245-251 (1991).

9. W. H. Prosser, K. E. Jackson, S. Kellas, B. T. Smith, J. McKeon, and A. Friedman, Advanced, Waveform Based Acoustic Emission Detection of Matrix Cracking in Composites, *Materials Evaluation* **53(9)**:1052-1058 (1995).

10. W. H. Prosser, The Propagation Characteristics of the Plate Modes of Acoustic Emission Waves in Thin Aluminum Plates and Thin Graphite/Epoxy Composite Plates and Tubes, *NASA Technical Memorandum 104187* (1991).

11. D. Guo, A. Mal, and K. Ono, Wave Theory of Acoustic Emission in Composite Laminates, *J. Acoustic Emission*, **14(3-4)**:S19-S46 (1996).

12. D. Guo, Lamb Waves from Microfractures in Composite Plates, *Ph. D. Thesis, University of California at Los Angeles* (1996).

13. M. R. Gorman and W. H. Prosser, Application of Normal Mode Expansion to Acoustic Emission Waves in Finite Plates, *J. Appl. Mech.*, **63(2)**:555-557 (1996).

14. R. D. Mindlin, Influence of Rotatory Inertia and Shear on Flexural Motions of Isotropic Elastic Plates, *J. Appl. Mech.*, **18**:31-38 (1951).

15. W. Huang, Application of Mindlin Plate Theory to Analysis of Acoustic Emission Waveforms in Finite Plates, to be published in the *Proceedings of the Review of Progress in Quantitative Nondestructive Evaluation*, **17** (1998).

16. J. Gary and M. A. Hamstad, On the Far-field Structure of Waves Generated by a Pencil Lead Break on a Thin Plate, *J. Acoustic Emission*, **12(3-4)**:157-170 (1994).

17. M. A. Hamstad, J. Gary, and A. O'Gallagher, Far-field Acoustic Emission Waves by Three-Dimensional Finite Element Modeling of Pencil-Lead Breaks on a Thick Plate, *J. Acoustic Emission*, **14(2)**:103-114 (1996).

18. P. C. Yang, C. H. Norris, and Y. Stavsky, Elastic Wave Propagation in Heterogeneous Plates, *Int. J. Solids Struct.* **2**:665 (1966)**.**

19. B. Tang, E. G. Henneke II, and R. C. Stiffler, Low Frequency Flexural Wave Propagation in Laminated Composite Plates, *Proceedings of Workshop on Acousto-Ultrasonics: Theory and Applications*, 45-65 (1987).

20. T. S. Chow, On the Propagation of Flexural Waves in an Orthotropic Laminated Plate and Its Response to an Impulsive Load, *J. Comp. Mat.*, **5**:306-319 (1971).

Table I. Properties of anisotropic material (unidirectional graphite/epoxy)used in DFEM model.

ρ	1550 kg/m^3
h	2.54 mm
c_{11}	147.1 GPa
c_{12}	4.11 GPa
$c_{13} = c_{12}$	4.11 GPa
c_{23}	3.09 GPa
c_{22}	10.59 GPa
$c_{33} = c_{22}$	10.59 GPa
$c_{44} = 1/2(c_{22} - c_{23})$	3.75 GPa
c_{55}	5.97 GPa
$c_{66} = c_{55}$	5.97 GPa

Table II. Properties of anisotropic material (unidirectional graphite/epoxy) used in MPT model.

ρ	1550 kg/m^3
h	2.54 mm
D_{11}	198.7 Pa·m^3
D_{22}	13.23 Pa·m^3
D_{12}	3.98 Pa·m^3
D_{66}	8.15 Pa·m^3
A_{44}	7.94 MPa·m
A_{55}	12.64 MPa·m

FIGURE CAPTIONS

Fig. 1 - Comparison of DFEM (solid curve) and MPT (dashed curve) results for isotropic (aluminum) material at propagation distances of (a) 7.62 cm, (b) 12.7 cm, and (c) 17.78 cm.

Fig. 2 - Comparison of DFEM (solid curve) and MPT (dashed curve) results for isotropic (aluminum) material at propagation distances of (a) 7.62 cm, (b) 12.7 cm, and (c) 17.78 cm on expanded time scales.

Fig. 3 - Comparison of DFEM (solid curve) and MPT (dashed curve) results for anisotropic (graphite/epoxy) material along 0° direction at propagation distances of (a) 7.62 cm and (b) 12.7 cm.

Fig. 4 - Comparison of DFEM (solid curve) and MPT (dashed curve) results for anisotropic (graphite/epoxy) material along 45° direction at propagation distances of (a) 7.62 cm and (b) 12.7 cm.

Fig. 5 - Comparison of DFEM (solid curve) and MPT (dashed curve) results for anisotropic (graphite/epoxy) material along 90° direction at propagation distances of (a) 7.62 cm and (b) 12.7 cm.

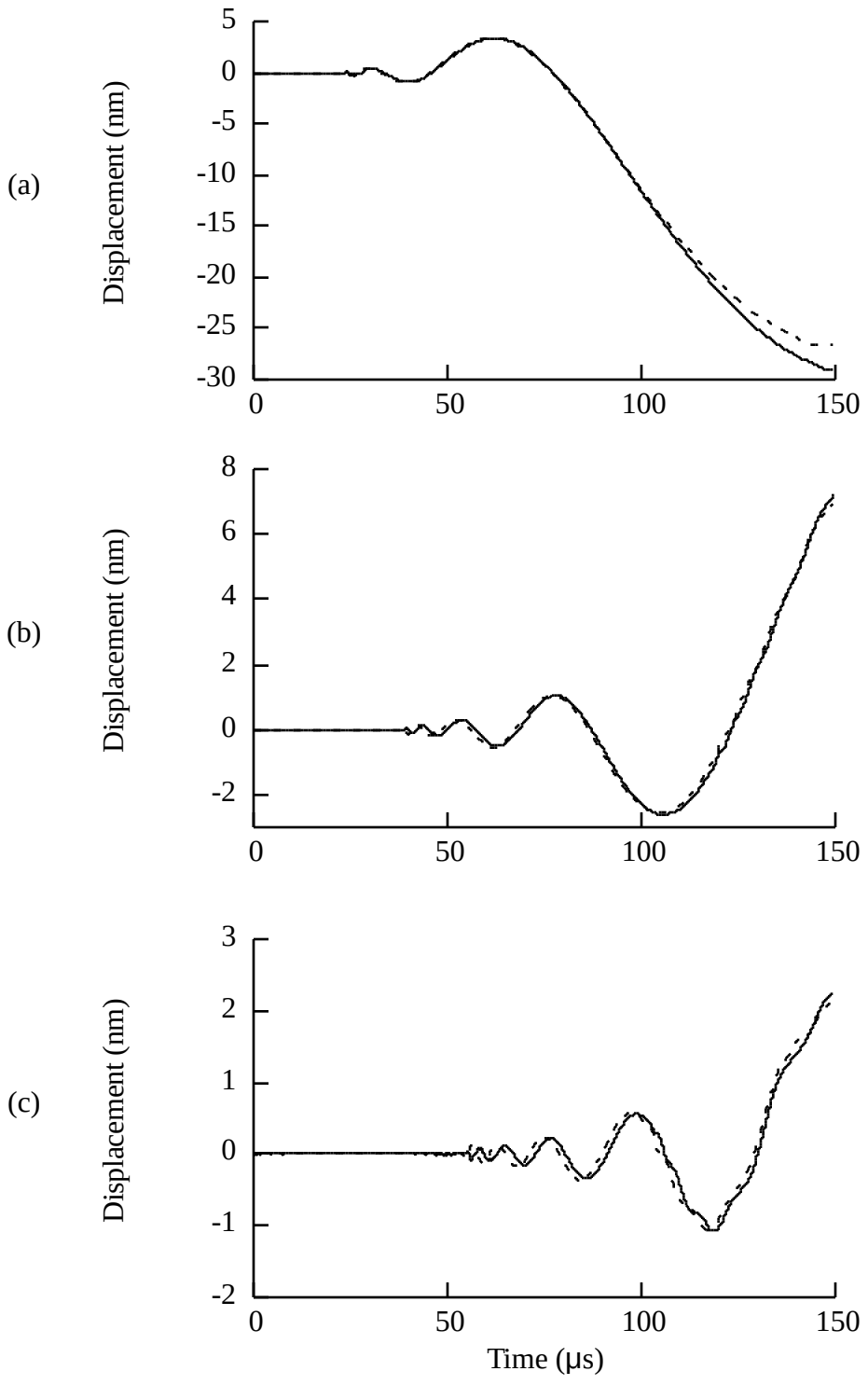
(a)
Displacement (nm)
5
0
-5
-10
-15
-20
-25
-30
0
50
100
150
(b)
Displacement (nm)
8
6
4
2
0
-2
0
50
100
150
(c)
Displacement (nm)
3
2
1
0
-1
-2
0
50
100
150
Time (μs)

Fig. 1

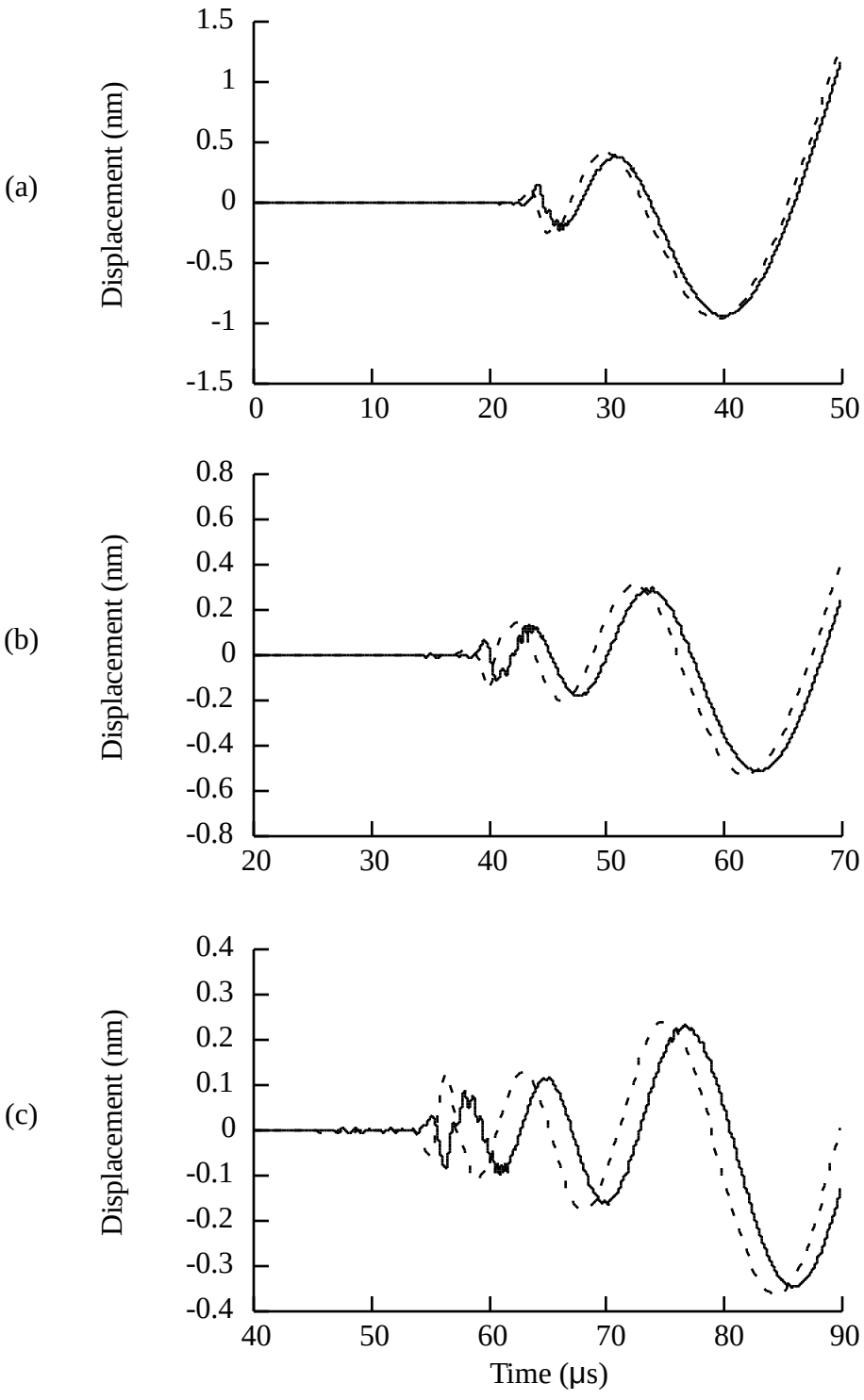
(a)
Displacement (nm)
1.5
1
0.5
0
-0.5
-1
-1.5
0
10
20
30
40
50
(b)
Displacement (nm)
0.8
0.6
0.4
0.2
0
-0.2
-0.4
-0.6
-0.8
20
30
40
50
60
70
(c)
Displacement (nm)
0.4
0.3
0.2
0.1
0
-0.1
-0.2
-0.3
-0.4
40
50
60
70
80
90
Time (μs)

Fig. 2

(a)

(b)

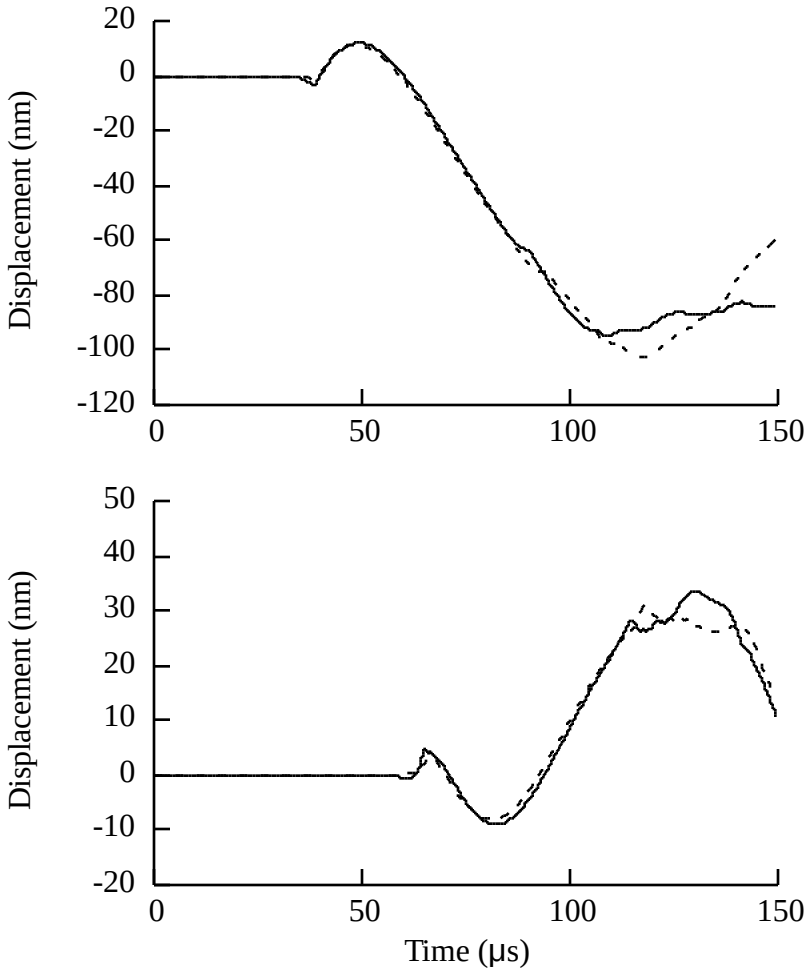
20
0
-20
-40
-60
-80
-100
-120
Displacement (nm)
0
50
100
150
50
40
30
20
10
0
-10
-20
Displacement (nm)
0
50
100
150
Time (μs)

Fig. 3

(a)

(b)

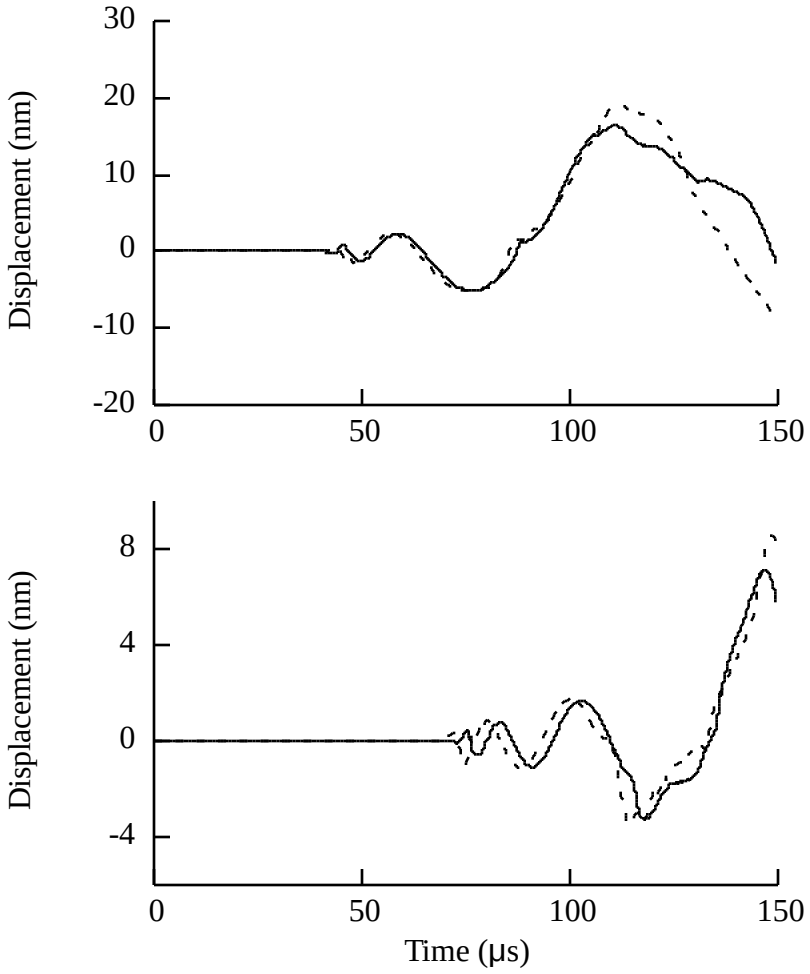
30
20
10
0
-10
-20
Displacement (nm)
0
50
100
150
8
4
0
-4
Displacement (nm)
0
50
100
150
Time (μs)

Fig. 4

(a)

(b)

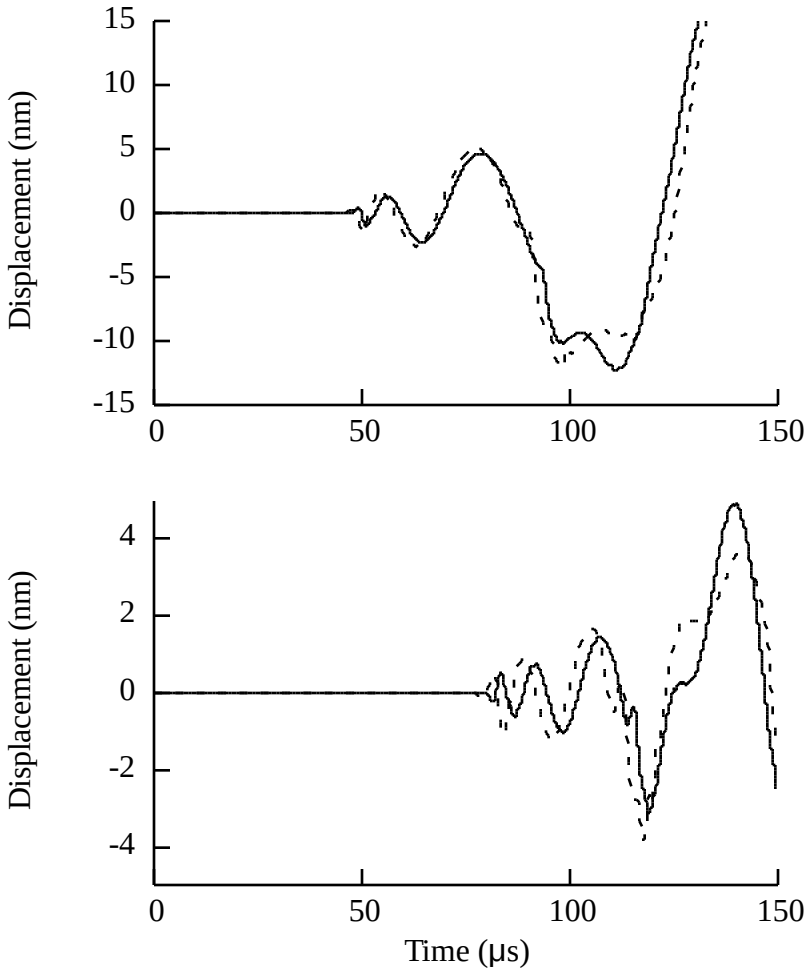
Displacement (nm)
15
10
5
0
-5
-10
-15
0
50
100
150
Displacement (nm)
4
2
0
-2
-4
0
50
100
150
Time (μs)

Fig. 5